

Isospin effects on the energy of vanishing flow in heavy-ion collisions

Sakshi Gautam¹, Rajiv Chugh¹, Aman D. Sood², Rajeev K. Puri¹,
Ch. Hartnack² and J. Aichelin²

¹*Department of Physics, Panjab University, Chandigarh -160 014, India.*

²SUBATECH,

Laboratoire de Physique Subatomique et des Technologies Associées

Université de Nantes - IN2P3/CNRS - EMN

4 rue Alfred Kastler, F-44072 Nantes, France.

June 20, 2018

Abstract

Using the isospin-dependent quantum molecular dynamics model we study the isospin effects on the disappearance of flow for the reactions of $^{58}\text{Ni}+^{58}\text{Ni}$ and $^{58}\text{Fe}+^{58}\text{Fe}$ as a function of impact parameter. We found good agreement between our calculations and experimentally measured energy of vanishing flow at all colliding geometries. Our calculations reproduce the experimental data within 5%(10%) at central (peripheral) geometries.

Electronic address: rkpuri@pu.ac.in

1 Introduction

The collective transverse in-plane flow [1–3] has been used extensively over the past three decades to study the properties of hot and dense nuclear matter, i.e. the nuclear matter equation of state (EOS) as well as the in-medium nucleon-nucleon (nn) cross section. This has been reported to be highly sensitive toward the above-mentioned properties as well as toward entrance channel parameters such as combined mass of the system [4–6], colliding geometries [7–11] as well as incident energy of the projectile [11–15]. The dependence of the collective flow on the above-mentioned parameters has revealed much interesting physics, especially the beam energy dependence which has also led to its disappearance. At lower incident energies, the dominance of the attractive mean field prompts the scattering of the particles into negative deflection angles thus producing negative flow whereas frequent nn collisions and repulsive mean field at higher incident energies result in the emission of particles into positive deflection angles and hence yield positive flow. While going through the incident energies, collective transverse in-plane flow disappears at a particular incident energy termed as the *balance energy* (E_{bal}) or *energy of vanishing flow* (EVF) [16]. The EVF has been studied experimentally as well as theoretically over a wide range of mass ranging from $^{12}C + ^{12}C$ to $^{238}U + ^{238}U$ at different colliding geometries and found to vary strongly as a function of the combined mass of the system [17–23] as well as a function of the impact parameter [10, 24–27].

At the same time the isospin degree of freedom plays an important role in heavy-ion collisions (HIC) through both nn collisions and the EOS. The later quantity is important because of its profound implications for studying the structure and evolution of many astrophysical objects such as neutron stars, supernova explosions, etc. To access the EOS as well as its isospin dependence, it is important to describe the observables of HIC such as collective transverse in-plane flow as well as its disappearance both of which in fact have been found to depend on the isospin degree of freedom. The first study showing the isospin effects on the collective flow and EVF was reported by Li *et al* [28], where a strong dependence of both the above-mentioned quantities was shown. The effect was found to be more pronounced at peripheral collisions. Later on, Pak *et al* [29] demonstrated experimentally the isospin effects on the collective flow and EVF at central and peripheral colliding geometries. The theoretical calculations using the isospin-dependent Boltzmann-Uehling-Uhlenbeck (IBUU) model were confronted with the data. The calculations under-predicted the experimentally measured EVF. Chen *et al* [30] studied the effect of the isospin degree of freedom on the collective flow and EVF using the isospin-dependent quantum molecular dynamics (IQMD) model, which was an improved version of the original QMD model [31, 32]. The calculated results were found to differ from the data at all colliding geometries. The reason for a large deviation was attributed to the low saturation density in the initialized nuclei which was about 0.12 fm^{-3} ($0.75 \rho_0$) as compared to the normal saturation density of 0.16 fm^{-3} and to the fact that the mean field due to the isospin-independent part of EOS would be more attractive at low density. However, it has been shown in [33] that the mean field potential is rather the same both at $\rho/\rho_0 = 1$ and 0.75 for the equations of state used in [30]. Only at values larger than ρ/ρ_0 , the mean field potential begins to differ. Moreover in [34] also, it has been shown that significant differences in the collective flow values due to the different initial densi-

ties occur only at high incident energies. These differences vanish in the EVF domain. Scalone *et al* [35] also studied the isospin effects on the collective flow. Their calculations indicate towards different neutron and proton flows (see [36] also). Their results of EVF were in good agreement with the data at $b/b_{max} = 0.45$. In this paper, we reproduce for the first time all the measured EVF for $^{58}Ni + ^{58}Ni$ and $^{58}Fe + ^{58}Fe$ systems (used to demonstrate isospin effect in [29] and [30]) and also explain in part why the calculations of [30] using the IQMD model show a large deviation from the measured EVF at all colliding geometries. For the present study, we use the IQMD model [34].

The IQMD model is an extension of the QMD model [31, 32], which treats different charge states of nucleons, deltas and pions explicitly, as inherited from the Vlasov-Uehling-Uhlenbeck (VUU) model [37]. The IQMD model has been used successfully for the analysis of a large number of observables from low to relativistic energies. The isospin degree of freedom enters into the calculations via symmetry potential, cross sections and Coulomb interaction.

In this model, baryons are represented by Gaussian-shaped density distributions

$$f_i(\vec{r}, \vec{p}, t) = \frac{1}{\pi^2 \hbar^2} \exp(-[\vec{r} - \vec{r}_i(t)]^2 \frac{1}{2L}) \times \exp(-[\vec{p} - \vec{p}_i(t)]^2 \frac{2L}{\hbar^2}) \quad (1)$$

Nucleons are initialized in a sphere with radius $R = 1.12 A^{1/3}$ fm, in accordance with the liquid-drop model. Each nucleon occupies a volume of h^3 , so that phase space is uniformly filled. The initial momenta are randomly chosen between 0 and Fermi momentum (\vec{p}_F). The nucleons of the target and projectile interact by two- and three-body Skyrme forces, Yukawa potential, Coulomb interactions and momentum dependent interactions. In addition to the use of explicit charge states of all baryons and mesons, a symmetry potential between protons and neutrons corresponding to the Bethe-Weizsacker mass formula has been included. The hadrons propagate using the Hamilton equations of motion:

$$\frac{d\vec{r}_i}{dt} = \frac{d\langle H \rangle}{d\vec{p}_i}; \quad \frac{d\vec{p}_i}{dt} = -\frac{d\langle H \rangle}{d\vec{r}_i} \quad (2)$$

with

$$\begin{aligned} \langle H \rangle &= \langle T \rangle + \langle V \rangle \\ &= \sum_i \frac{p_i^2}{2m_i} + \sum_i \sum_{j>i} \int f_i(\vec{r}, \vec{p}, t) V^{ij}(\vec{r}', \vec{r}) \\ &\quad \times f_j(\vec{r}', \vec{p}', t) d\vec{r}' d\vec{p}' \end{aligned} \quad (3)$$

The baryon potential V^{ij} , in the above relation, reads as

$$\begin{aligned} V^{ij}(\vec{r}' - \vec{r}) &= V_{Skyrme}^{ij} + V_{Yukawa}^{ij} + V_{Coul}^{ij} + V_{mdi}^{ij} + V_{sym}^{ij} \\ &= [t_1 \delta(\vec{r}' - \vec{r}) + t_2 \delta(\vec{r}' - \vec{r}) \rho^{\gamma-1} (\frac{\vec{r}' + \vec{r}}{2})] \\ &\quad + t_3 \frac{\exp(-|\vec{r}' - \vec{r}|/\mu)}{(|\vec{r}' - \vec{r}|/\mu)} + \frac{Z_i Z_j e^2}{|\vec{r}' - \vec{r}|} \\ &\quad + t_4 \ln^2 [t_5 (\vec{p}' - \vec{p})^2 + 1] \delta(\vec{r}' - \vec{r}) \\ &\quad + t_6 \frac{1}{\rho_0} T_{3i} T_{3j} \delta(\vec{r}' - \vec{r}). \end{aligned} \quad (4)$$

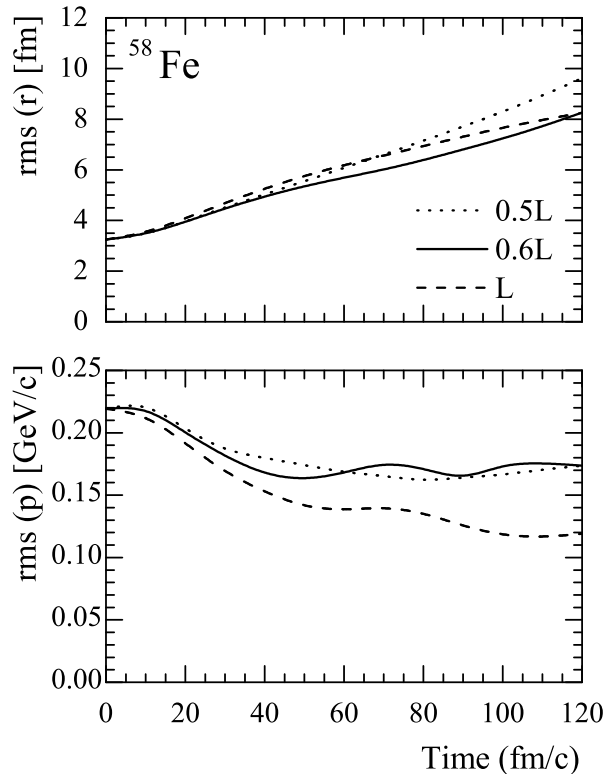


Figure 1: Time evolution of root mean square radii of a single ^{58}Fe nucleus in coordinate and momentum space obtained with IQMD for EOS used in the present study for different Gaussian widths of 0.5L, 0.6L and L. Various lines are explained in the text.

Here $t_6 = 4C$ with $C = 32$ MeV and Z_i and Z_j denote the charges of the i th and j th baryon, and T_{3i} and T_{3j} are their respective T_3 components (i.e. $1/2$ for protons and $-1/2$ for neutrons). The parameters μ and t_1, \dots, t_6 are adjusted to the real part of the nucleonic optical potential. For the density dependence of the nucleon optical potential, standard Skyrme-type parametrization is employed. The momentum dependence V_{mdi}^j of the nn interactions, which may optionally be used in IQMD, is fitted to the experimental data in the real part of the nucleon optical potential. We also use the standard energy-dependent free nn cross section σ_{nn}^{free} as well as the cross section reduced by 20%, i.e. $\sigma = 0.8 \sigma_{nn}^{free}$. The details about the elastic and inelastic cross sections for proton-proton and proton-neutron collisions can be found in [34, 38]. The cross sections for neutron-neutron collisions are assumed to be equal to the proton-proton cross sections. Two particles collide if their minimum distance d fulfills

$$d \leq d_0 = \sqrt{\frac{\sigma_{tot}}{\pi}}, \sigma_{tot} = \sigma(\sqrt{s}, type), \quad (5)$$

where 'type' denotes the ingoing collision partners (N-N...). Explicit Pauli blocking is also included; i.e. Pauli blocking of the neutrons and protons is treated separately. We assume that each nucleon occupies a sphere in coordinate and momentum space. This

trick yields the same Pauli blocking ratio as an exact calculation of the overlap of the Gaussians will yield. We calculate the fractions P_1 and P_2 of final phase space for each of the two scattering partners that are already occupied by other nucleons with the same isospin as that of scattered ones. The collision is blocked with the probability

$$P_{block} = 1 - [1 - \min(P_1, 1)][1 - \min(P_2, 1)], \quad (6)$$

and, correspondingly is allowed with the probability $1 - P_{block}$. For a nucleus in its ground state, we obtain an averaged blocking probability $\langle P_{block} \rangle = 0.96$. Whenever an attempted collision is blocked, the scattering partners maintain the original momenta prior to scattering. As mentioned in [34], in IQMD the Gaussian width L (which can be regarded as a description of the interaction range of the particle) depends on the system under study. The system dependence of L in IQMD has been introduced in order to obtain the maximum stability of the nucleonic density profile. For example, for Au+Au (Ca+Ca and lighter nuclei) $L = 2.16$ (1.08) fm^2 . Therefore, in the present study we use the Gaussian width $0.6L$. In figure 1 we display the time evolution of the rms radius of a single ^{58}Fe nucleus in coordinate and momentum space for different choices of L . The dotted, solid and dashed lines are for the Gaussian width $0.5L$, $0.6L$ and L , respectively. From the figure, we see that ^{58}Fe shows the maximum stability for the Gaussian width $0.6L$ and is least stable for $0.5L$. We also find that the stability of a single ^{58}Fe nucleus is quite the same for $0.6L$ and L . We find similar results for the ^{58}Ni nucleus also (not shown here). We will come back to this point later. It is worth mentioning that the appropriate choice of the Gaussian width (interaction range) is very important since a choice of a different interaction range causes different density profiles of the ground-state nucleus which results in the different strengths of density gradient that in turn has strong influence on the variables such as flow, multifragmentation, pion, kaon production etc [34, 39, 40].

We simulate 2500 events for the reactions $^{58}Ni + ^{58}Ni$ and $^{58}Fe + ^{58}Fe$ between incident energy range from 50 to 150 MeV/nucleon in small steps of 10 MeV/nucleon. The impact parameters are guided by [29]. We use the soft EOS along with momentum-dependent interactions (MDI) labeled as SMD. The reactions are followed till the transverse flow saturates. The saturation time is around 100 fm/c for the reactions in the present study. There are several methods in the literature to define the nuclear transverse in-plane flow. In most of the studies, the EVF is extracted from (p_x/A) plots where one plots (p_x/A) as a function of $Y_{c.m.}/Y_{beam}$. Using the linear fit to the slope, one can find the so-called reduced flow F . Naturally, the energy at which the reduced flow passes through zero is called the EVF. Alternatively, one can also use a more integrated quantity "directed transverse momentum $\langle p_x^{dir} \rangle$ " which is defined as [23, 31, 34, 41]

$$\langle p_x^{dir} \rangle = \frac{1}{A} \sum_{i=1}^A \text{sign}\{y(i)\} p_x(i), \quad (7)$$

where $y(i)$ and $p_x(i)$ are, respectively, the rapidity and the momentum of the i^{th} particle. The rapidity is defined as

$$Y(i) = \frac{1}{2} \ln \frac{\vec{E}(i) + \vec{p}_z(i)}{\vec{E}(i) - \vec{p}_z(i)}, \quad (8)$$

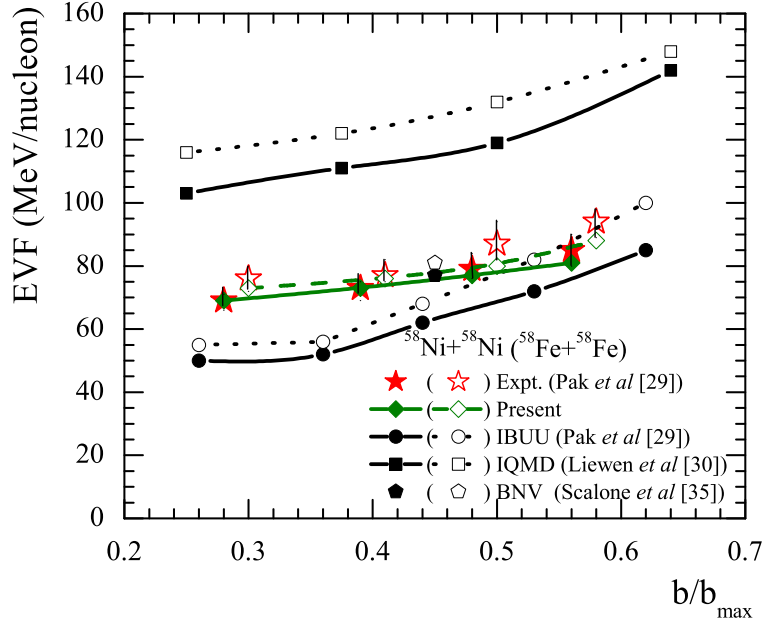


Figure 2: The EVF as a function of the reduced impact parameter. Various symbols are explained in the text

where $\vec{E}(i)$ and $\vec{p}_z(i)$ are, respectively, the energy and longitudinal momentum of the i^{th} particle. In this definition, all the rapidity bins are taken into account. It, therefore, presents an easier way to measure the in-plane flow rather than complicated functions such as $\langle p_x/A \rangle$ plots. It has been shown in [23] that the disappearance of flow occurs at the same incident energy in both the cases showing the equivalence between p_x/A and $\langle p_x^{dir} \rangle$ as far as the EVF is concerned. It is worth mentioning that the EVF has the same value for all fragments types [18, 26, 29, 42, 43]. Further the apparatus corrections and acceptance do not play any role in calculation of the EVF [4, 18, 43].

In figure 2, we display the EVF as a function of the reduced impact parameter b/b_{max} for the reactions $^{58}Ni + ^{58}Ni$ (solid symbols) and $^{58}Fe + ^{58}Fe$ (open symbols). Stars represent the experimental data whereas diamonds correspond to our theoretical calculations. Squares (circles) represent the IQMD (IBUU) calculations of [30] ([29]). Pentagons represent the theoretical calculations of [35] for $b/b_{max} = 0.45$. The lines are only to guide the eye. Our results of the EVF and experimental data for the reaction $^{58}Fe + ^{58}Fe$ have been slightly offset in the horizontal direction for clarity. The vertical lines on the data points represent statistical errors. The statistical error bars on theoretical points of [29] and [30] are not displayed, again for clarity. For the calculations of EVF, we use the standard energy-dependent free nn cross section as was done in [29] and [30] also. Our EVF values for σ_{nn}^{free} (not shown here) are lower than the data consistently by about 25%, at all colliding geometries. Therefore, we reduce the cross section by 20% with $\sigma = 0.8\sigma_{nn}^{free}$. We find that the EVF increases with decrease in cross section at all colliding geometries in agreement with [23] where Sood and Puri have decomposed the

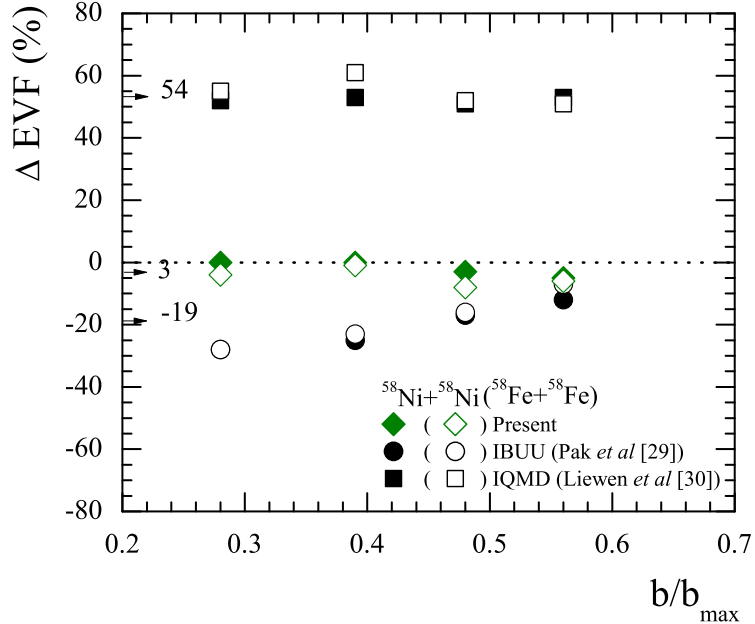


Figure 3: The percentage deviation of EVF values for different calculations over the experimentally measured EVF as a function of the reduced impact parameter.

total transverse flow into contribution due to mean field and two-body collision parts and showed that the EVF is a result of counterbalancing of the flow due to mean field and collisions. With a decrease in cross section, the flow due to collisions decreases; therefore, higher incident energy is needed to compensate this effect. From the figure we see that our calculations are in good agreement with the data and the calculations of [35]. Note that we have also used symmetry energy linear in its density dependence as was done in [29] and [30]. The results of IBUU calculations [29] under-predict the data whereas the IQMD calculations of [30] over-predict the data consistently. It is worth mentioning here that the choice of reduced cross section has also been motivated by [45] as well as many previous studies [6, 15, 20, 46, 47]. In [45], Daffin and Bauer have suggested the factor of 0.2-0.3 for the density-dependent reduction of the in-medium cross section. Their theoretical results (not shown here) were much closer to the data when using the in-medium reduction of the scattering cross section. However the difference between EVF of $^{58}\text{Fe} + ^{58}\text{Fe}$ and $^{58}\text{Ni} + ^{58}\text{Ni}$, at all colliding geometries, was reduced by a factor of 4 than what was observed in experiments. Further, we have calculated the EVF at central and peripheral colliding geometries with the isotropic cross section. We find the effect of an angular distribution of the scattering cross sections on the EVF to be negligible for both $^{58}\text{Fe} + ^{58}\text{Fe}$ and $^{58}\text{Ni} + ^{58}\text{Ni}$. It is worth mentioning here that the effect of an angular distribution on transverse flow is significant at higher energies [44]. We have also calculated the EVF for neutrons and protons for the more neutron-rich system where a larger difference between neutron and proton flow is expected [35]. We find that the EVF is the same for neutrons, protons and all nucleons at central collisions. At peripheral collisions, neutron and proton EVF

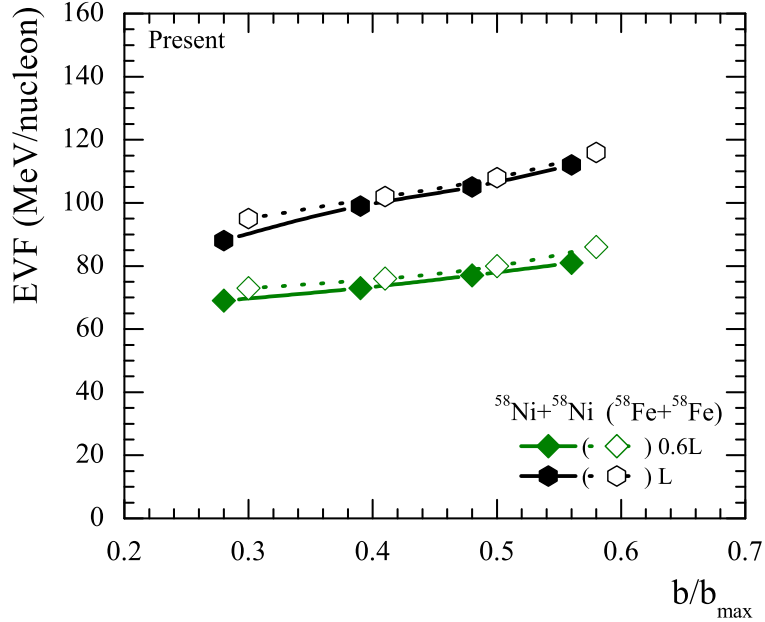


Figure 4: The EVF as a function of the reduced impact parameter for different values of L . The solid (open) symbols represent the reactions $^{58}\text{Ni} + ^{58}\text{Ni}$ ($^{58}\text{Fe} + ^{58}\text{Fe}$). Hexagons (diamonds) correspond to L ($0.6L$). The lines are only to guide the eye.

differ each other by 3 MeV and the EVF for all nucleons lie in between the neutron and proton EVF. The results are in agreement with [35]. Further, we have checked the effect of different symmetry energy (by varying both the strength of symmetry energy as well as its density dependence) on the transverse flow (due to neutrons, protons and all nucleons) at high densities. At 150 MeV/nucleon, although we obtain different neutron and proton flow in agreement with [35], the difference between neutron and proton flow is insensitive to the choice of symmetry energy for the systems in the present study. However, we do not exclude the possibility of this effect for systems having a large N/Z ratio. At 400 MeV/nucleon the transverse flow is insensitive to the symmetry energy. In the present study the effect of n/p effective mass splitting is expected to be negligible since N/Z ratio for the two systems in the present study is small. The above discussion indicates that the studies with systems having a large difference between the N/Z ratio in the Fermi energy domain could be best suitable to explore the isospin effects of in-medium nuclear interactions in transverse flow.

In figure 3, we show the percentage deviation ΔEVF (%) of the calculated EVF over experimental data with $\Delta EVF(\%) = \frac{EVF_{theo} - EVF_{expt}}{EVF_{expt}} \times 100$. The symbols have same meaning as in figure 2. In the case of IBUU calculations, percentage deviation for central collisions is about 28%, whereas for peripheral collisions it is about 10%. The average deviation is about 19% over all colliding geometries. In the case of IQMD calculations of [30], we see that the percentage deviation ΔEVF (%) is about 55% at all geometries, i.e. the calculated EVF are consistently higher compared to the data. As mentioned

previously and in [34], in IQMD the system-dependent width of the Gaussian is used to achieve the maximum stability of the nucleus. It has also been shown in [34, 39] that the collective flow and EVF depend strongly on the interaction range of the particle. The higher the interaction range, the smaller is the collective flow and therefore larger is the EVF. In IQMD calculations of [30], the interaction range was taken to be 2 fm^2 which in part could have led to the reduction of flow and enhancement of EVF consistently at all colliding geometries. For our calculations, we use the interaction range $0.6L$. We find good agreement with the experimental data at all colliding geometries. It is worth mentioning here that the treatment of various potential terms such as Yukawa, Coulomb and MDI is quite similar in our IQMD model and the IQMD model of Chen *et al* [30]. Although in our model the range of Yukawa force is 0.4 fm as compared to 1.2 fm in the IQMD model of Chen, it has been shown in [34] that the Yukawa forces have insignificant effects on collective flow. The treatment of the asymmetry term is also similar in both the models with $C = 32 \text{ MeV}$. Moreover, Pauli blocking is also treated similarly in both the models. To further strengthen our point, we therefore took the interaction range L in our IQMD model and found a huge enhancement in the calculated EVF making our calculations close to that of [30] as shown in figure 4. It should be noted here that although both ^{58}Fe and ^{58}Ni nuclei (see figure 1 and text) show quite similar stability for Gaussian widths $0.6L$ and L , the EVF values for the two different choices of Gaussian width are quite different. This also indicates that the choice of Gaussian width affects the collective flow and EVF quite strongly which is in agreement with [34, 39].

In Summary, using the IQMD model, we have studied the isospin effects on the disappearance of flow for the reactions $^{58}\text{Ni} + ^{58}\text{Ni}$ and $^{58}\text{Fe} + ^{58}\text{Fe}$ (for which data are available) at all colliding geometries. We have found good agreement of our calculations with the data at all colliding geometries. Our calculations explain the data within 5% (10%) at central (peripheral) collisions. We also find that the EVF is affected strongly by the choice of Gaussian width. We are also able to explain, in part, the large deviation of the results of [30] from data by the choice of a large width of the Gaussian.

Acknowledgments

One of the authors, ADS would like to thank Indian Physics Association for giving national award for Ph.D thesis in 2006. This work is supported by Indo-French project no. 4104-1.

References

- [1] Scheid W, Müller H and Greiner W 1974 *Phys. Rev. Lett.* **32** 741
- [2] Gustafsson H A *et al* 1984 *Phys. Rev. Lett.* **52** 1590
- [3] Doss K G R *et al* 1986 *Phys. Rev. Lett.* **57** 302
- [4] Ogilvie C A *et al* 1989 *Phys. Rev. C* **40** 2592
- [5] Blättel B *et al* 1991 *Phys. Rev. C* **43** 2728
- [6] Andronic A *et al* 2003 *Phys. Rev. C* **67** 034907
- [7] Pan Q and Danielewicz P 1993 *Phys. Rev. Lett.* **70** 2062

- [8] Ramillien V *et al* 1995 *Nucl. Phys. A* **587** 802
- [9] Bertsch G F, Lynch W G and Tsang M B 1987 *Phys. Lett. B* **189** 384
- [10] Lukasik J *et al* 2005 *Phys. Lett. B* **608** 223
- [11] Zhang Y and Li Z 2006 *Phys. Rev. C* **74** 014602
- [12] Zhang W M *et al* 1990 *Phys. Rev. C* **42** R491
- [13] Beavis D *et al* 1992 *Phys. Rev. C* **45** 299
- [14] Lukasik J and Trautmann W 2008 arxiv-0708.2821V1
- [15] Hong B *et al* 2000 *Phys. Rev. C* **66** 034901
- [16] Krofcheck D *et al* 1989 *Phys. Rev. Lett.* **63** 2028
- [17] Mota V de la, Sebille F, Farine M, Remaud B and Schuk P 1992 *Phys. Rev. C* **46** 677
- [18] Westfall G D *et al* 1993 *Phys. Rev. Lett.* **71** 1986
- [19] Zhou H, Li Z and Zhuo Y 1994 *Phys. Rev. C* **50** R2664
- [20] Zhou H, Li Z, Zhuo Y and Mao G 1994 *Nucl. Phys.* **A580** 627
- [21] Majestro D J *et al* 2000 *Phys. Rev. C* **61** 021602(R)
- [22] Majestro D J, Bauer W and Westfall G D 2000 *Phys. Rev. C* **62** 041603(R)
- [23] Sood A D and Puri R K 2004 *Phys. Rev. C* **69** 054612
Sood A D and Puri R K 2004 *Phys. Lett. B* **594** 260
Sood A D and Puri R K 2006 *Eur. Phys. J. A* **30** 57
Sood A D and Puri R K 2006 *Phys. Rev. C* **73** 067602
- [24] Sullivan J P *et al* 1990 *Phys. Lett. B* **249** 8
- [25] Buta A *et al* 1995 *Nucl. Phys.* **A584** 397
- [26] Pak R *et al* 1996 *Phys. Rev. C* **53** R1469
- [27] Chugh R and Puri R K 2010 *Int. J. Mod. Phys. E* (in press).
- [28] Li B A, Ren Z, Ko C M and Yennello S J 1996 *Phys. Rev. Lett.* **76** 4492
- [29] Pak R *et al* 1997 *Phys. Rev. Lett* **78** 1022
Pak R *et al* 1997 *Phys. Rev. Lett.* **78** 1026
- [30] Liewen C, Fengshou Z and Genming J 1998 *Phys. Rev. C* **58** 2283
- [31] Aichelin J 1991 *Phys. Rep.* **202** 233.

- [32] Singh J, Kumar S and Puri R K 2000 *Phys. Rev.C* **62** 044617
 Puri R K and Aichelin J 2000 *J. Comput. Phys.* **162** 245
 Kumar S, Puri R K and Aichelin J 1998 *Phys. Rev. C* **58** 1618
 Vermani Y K *et al* 2010 *J. Phys. G: Nucl. Part. Phys.* **37** 015105
 Vermani Y K, Goyal S, and Puri R K 2009 *Phys. Rev. C* **79** 064613
 Vermani Y K and Puri R K 2009 *Eur. Phys. Lett.* **85** 62001
 Sood A D and Puri R K 2009 *Phys. Rev. C* **79** 064618
- [33] Khoa D T *et al* 1992 *Nucl. Phys.* **A548** 102
- [34] Hartnack C, Puri R K, Aichelin J, Konopka J, Bass S A, Stöcker H and Greiner W
 1998 *Eur. Phys. J A* **1** 151
- [35] Scalone L, Colonna M and Di Toro M 1999 *Phys. Lett. B* **461** 9
- [36] Baran V, Colonna M, Greco V and Di Toro M 2005 *Phys. Rep.* **410** 335
 Li B A, Chen L W and Ko C M 2008 *Phys. Rep.* **464** 113
- [37] Kruse H, Jacak B V and Stöcker H 1985 *Phys. Rev. Lett.* **54** 289
 Molitoris J J and Stöcker H 1985 *Phys. Rev. C* **32** 346 (R)
- [38] Cugnon J, Mizutani T and Vandermeulen J 1981 *Nucl. Phys.* **A352** 505
- [39] Klakow D, Welke G and Bauer W 1993 *Phys. Rev. C* **48** 1982
- [40] Hartnack C, Jaenicke J, Sehn L, Stöcker H and Aichelin J 1994 *Nucl. Phys.* **A580**
 643
- [41] Lehmann E, Faessler A, Zipprich J, Puri R K and Huang S W 1996 *Z. Phys. A* **355**
 55
- [42] Westfall G D 1998 *Nucl. Phys.* **A630** 27c
- [43] Cussol D *et al* 2002 *Phys. Rev. C* **65** 044604
- [44] Hartnack C 1989 MPhil Thesis Institut für Theoretische Physik Universität Frankfurt am Main
- [45] Daffin F and Bauer W 1998 arxiv: nucl-th/9809024v1
- [46] Peter J 1992 *Nucl. Phys.* **A545** 173c
- [47] Ono A, Horiuchi H and Maruyama T 1993 *Phys. Rev. C* **48** 2946